Macromolecules
ARTICLE

Macromolecules **2010**, *43*, 4843–4852 **4843**
DOI: 10.1021/ma100957q

Preparation of Nanoporous Poly(3-hexylthiophene) Films Based on a Template System of Block Copolymers via Ionic Interaction

Ayumi Takahashi,[†,§] Yecheol Rho,[‡,§] Tomoya Higashihara,*[,†] Byungcheol Ahn,[‡] Moonhor Ree,*[,‡] and Mitsuru Ueda*[,†]

[†]*Department of Organic and Polymeric Materials, Graduate School of Science and Engineering, Tokyo Institute of Technology, 2-12-1-H-120, O-okayama, Meguro-Ku, Tokyo, 152-8552, Japan, and* [‡]*Department of Chemistry, Center for Electro-Photo Behaviors in Advanced Molecular Systems, BK School of Molecular Science, Division of Advanced Materials Science, and Polymer Research Institute, Pohang University of Science & Technology (POSTECH), Pohang 790-784, Republic of Korea.* [§]*These authors equally contributed to this work*

Received February 16, 2010; Revised Manuscript Received May 3, 2010

ABSTRACT: A series of well-defined aniline-chain-end-functionalized regioregular poly(3-hexylthiophene)s (P3HT−NH_2) and sulfo-chain-end-functionalized polystyrene (PS−SO_3H) have been prepared based on quasi-living Grignard metathesis and living anionic polymerization, respectively. Block copolymers via ionic interaction, (P3HT−NH_3^+)-*b*-(PS−SO_3^-)s, were successfully synthesized, simply by blending P3HT−NH_2 with PS−SO_3H in toluene. The thermal and optical properties of the block copolymers were investigated by differential scanning calorimetry (DSC) and ultraviolet−visible (UV−vis) spectroscopy. The self-assembly behavior of the (P3HT−NH_3^+)-*b*-(PS−SO_3^-) thin film was observed by atomic force microscopy (AFM) and transmission electron microscopy (TEM). In addition, grazing incidence X-ray scattering (GIXS) analysis found the microphase separation of P3HT−NH_3^+ and PS−SO_3^- domains as well as the packing behavior of P3HT−NH_3^+ segments in block copolymer thin films. By exploiting the pH-sensitive ionic interaction, the PS−SO_3^- domains were selectively etched with ethyl acetate/triethylamine, cleaving the ionic interaction between P3HT−NH_3^+ and PS−SO_3^- segments, to obtain the target nanoporous P3HT−NH_2 films. The porosity of the films was confirmed by AFM, scanning electron microscopy (SEM) and GIXS analyses.

Introduction

Thin films of block copolymers can self-assemble into many types of highly ordered nanostructures on substrates after being cast from a number of solvents.[1−6] Selective etching of one of the domains after self-assembly leads to nanoporous films that are useful for separations and templates in nanotechnology.[7−10] Among them, nanoporous regioregular poly(3-hexylthiophene) (P3HT) films derived from a block copolymer template are quite interesting and are expected to be used for such applications as voltaic chemical sensors and, in particular, bulk-heterojunction (BHJ) organic photovoltaic cells,[11,12] after performing a backfill of *n*-type semiconductors into the porous P3HT films. Because of large *p*/*n* interface areas and well-connected charge transporting channels having widths comparable to exciton diffusion lengths (∼10 nm), efficient charge separation with less recombination and fast charge transport are expected, resulting in high power conversion efficiency.

Hillmyer and co-workers reported nanoporous P3HT films for the first time by using a template of a block copolymer of P3HT and poly(D,L-lactide) (PLA) segments.[13] Starting from *ω*-chain-end-vinyl-functionalized P3HT, the chain end was transformed into a hydroxy group, followed by controlled ring-opening polymerization of D,L-lactide from an aluminum alkoxide macro-initiator to synthesize P3HT-*b*-PLA. After etching the P3HT-*b*-PLA films with an alkaline solution, the target nanoporous P3HT films were successfully created. A backfill of water-soluble fullerene derivatives into a similar nanoporous P3HT film, derived from P3HT-*b*-PLA, was recently performed by a different group to create an ideal *p*/*n* BHJ active layer, however, the characterization of the photovoltaic cells was not shown.[14] Hawker and co-workers recently reported the creation of nanoporous P3HT films by selective solvent etching of PS segments after being cleaved off from a template of P3HT grafted with polystyrene (PS) segments via a trityl ether linkage.[15] However, the morphology of porous sites may be different from that using P3HT-*b*-PLA as a template, because the topological structure of the template polymer was not a linear block.

Nano-ordered microphase separation of P3HT-based rod−coil block copolymer films has recently been clarified, similar to a conventional coil−coil block copolymer, induced by spontaneous self-assembly of each immiscible segment in which domains rich in one block are separated from domains rich in the other so as to minimize contact energy. Indeed, McCullough and co-workers observed the nanofibril structures of P3HT-*b*-PS,[16] P3HT-*b*-polyisoprene,[16] and P3HT-*b*-poly(methacrylate)[17] by atomic force microscopy (AFM). We also found similar nanofibril structures 12−15 nm in width in thin films of PS−*b*-P3HT-*b*-PS,[18] poly(4-vinyltriphenylamine)(P4VTPA)-*b*-P3HT-*b*-P4VTPA,[19] and poly(methyl methacrylate)(PMMA)-*b*-P3HT-*b*-PMMA triblock copolymers.[20] Recently, Dai and co-workers reported clear sphere, cylinder, and lamellar structures of a P3HT-*b*-P2VP film, depending on composition.[21]

Although these studies utilizing covalently bonded block copolymers are presently very numerous, the synthesis of ion-bonded block copolymers, by a blend system of two different chain-end-functionalized polymers, showing similar nanostructures, has

*To whom correspondence should be addressed. E-mail: thigashihara@polymer.titech.ac.jp (T.H.), ree@postech.edu (M.R.), ueda.m.ad@m.titech.ac.jp (M.U.). Telephone: +81-3-5734-2126. Fax: +81-3-5734-2126.

Published on Web 05/14/2010

scarcely been focused on yet. The advantages of using such a system are as follows: (1) more facile synthetic approaches are available for chain-end-functionalized polymers than for block copolymers, (2) the combination of block segments is versatile without component limitations, as seen in covalently bonded block copolymers, (3) there is a possibility of creating nanoporous films by selective solvent etching of one of the segments after cleaving the ionic bonds under acidic or alkaline conditions.

In the course of previous studies on the synthesis and self-assembly of ion-bonded block copolymers,[22−26] only conventional segments were employed and π-conjugated polymer segments have never been used. Recently, Hirao and co-workers reported the synthesis of block and star-branched copolymers consisting of polyacetylene rods and other coil segments via ionic interaction.[27,28] They used blends between chain-end- or in-chain-functionalized (PS)s with carboxy groups and chain-end- or in-chain-functionalized poly(phenyl vinyl sulfoxide)s with *N,N*-dimethylamino groups which were transformed into polyacetylenes by a thermal treatment eliminating sulfenic acids. However, the insolubility and low oxidative stability of the resulting material seem to be problematic for practical device application.

Herein we demonstrate the preparation of nanoporous P3HT films by a template system of a novel P3HT-based block copolymer via ionic interaction, (P3HT−NH_3^+)-*b*-(PS−SO_3^-), prepared by blending an aniline-chain-end-functionalized P3HT (P3HT−NH_2) and a sulfo-chain-end-functionalized PS (PS−SO_3H). Since both polymers are prepared by quasi-living GRIM and living anionic polymerization, respectively, they possess predictable molecular weights and quite low polydispersity indices (PDIs), and thereby well-defined self-organizing nanostructures could be expected from their blend films.

Experimental Section

Materials. All chemicals (> 98%) were purchased from Aldrich, Japan and used as received unless otherwise stated. Tetrahydrofuran (THF) was refluxed over sodium benzophenone for 12 h and then distilled. Styrene was washed with a 5% NaOH aqueous solution, and dried over $MgSO_4$. After filtration, it was distilled from CaH_2 under the reduced pressure. Toluene for living anionic polymerization was washed with H_2SO_4, neutralized with a 5% NaOH aqueous solution, washed with water, and dried over $CaCl_2$. It was further dried over P_2O_5, and finally distilled from 1,1-diphenylhexyllithium. 2-Bromo-3-hexyl-5-iodobenzene (**1**) was prepared according to a previous paper.[29]

Synthesis of Regioregular P3HT−NH_2. The representative synthetic procedure is described as follows. In a three-neck 30 mL flask, lithium chloride (LiCl, 0.17 g, 4.01 mmol) was placed and dried at 150 °C for 30 min. After cooling to room temperature and purging with dry nitrogen, freshly distilled **1** (0.313 g, 0.839 mmol) was charged and pumped up for 15 min. After purging again with dry nitrogen, dry THF (15 mL) was added and cooled to 0 °C for 30 min with stirring. A THF solution of isopropylmagnesium chloride (^{i}PrMgCl, 2 M × 0.460 mL = 0.92 mmol) was then added and kept at 0 °C for additional 30 min to prepare the monomer, 2-bromo-5-chloromagnesio-3-hexylthiophene (**2**). In the separate three neck 10 mL flask, diphenylphosphinopropanenickel(II) dichloride (Ni(dppp)Cl_2, 17 mg, 0.0314 mmol) was charged, pumped up for 15 min with stirring, and purged with dry nitrogen. Dry THF (5 mL) was then added to prepare the suspension solution of Ni(dppp)Cl_2. This solution was added to the monomer solution at once with vigorous stirring adjusted at 700 rpm at room temperature. After the polymerization for 10 min, a THF solution of 3-[bis(trimethylsilyl)amino]phenylmagnesium chloride (**3**, 1 M × 1.5 mL = 1.5 mmol) was added and stirred for 10 min, followed by quenching with 5 N HCl (2 mL). The mixture solution was poured into water/methanol (3/7, v/v, 200 mL) to precipitate the polymer. The soxleht extraction was performed using methanol, acetone, and chloroform. Then, a chloroform solution of the polymer was washed with $NaHCO_3$(aq) three times and poured again into water/methanol (3/7, v/v, 200 mL) to precipitate the polymer. It was finally freeze-dried from the benzene solution to afford regioregular P3HT−NH_2. Monomer conversion: 98%. Isolation yield: 182 mg, 76%. $\overline{M}_n$(number-average molecular weight): 7530. PDI: 1.11. Regioregularity: 95%. Aniline functionality: 90%.

Synthesis of PS−SO_3H. Styrene (3.11 g, 0.0299 mmol) was polymerized with *sec*-BuLi (1.07 M x 0.290 mL = 0.310 mmol) in toluene (12 mL) at room temperature for 2 h under a dry argon atmosphere. After cooling the system to −78 °C, a THF (15 mL) solution of 1,1-diphenylethylene (DPE, 0.938 mmol) was added and stirred for 30 min. Then, 1,3-propane sultone (0.068 mL, 0.77 mmol) was added to the solution at −78 °C, followed by standing for another 30 min. The resulting solution was poured in methanol (300 mL) to precipitate the polymer. It was again dissolved in THF and neutralized with a hydroperchloric acid aqueous solution. After reprecipitation from THF to methanol twice, the polymer was purified silca-gel flash column chromatography using toluene and THF as eluents. It was freeze-dried from its absolute benzene solution twice. Isolation yield: 100%. $\overline{M}_n$: 12 500. PDI: 1.03. Sulfo-functionality: 100%.

Synthesis of (P3HT−NH_3^+)-*b*-(PS−SO_3^-). In a typical experiment, an equimolar of P3HT−NH_2 ($\overline{M}_n$: 7530, PDI: 1.11, 3.8 mg, 5.1×10^{-4} mmol) and PS−SO_3H ($\overline{M}_n$: 12 500, PDI: 1.03, 6.4 mg, 5.1×10^{-4} mmol) were dissolved in toluene (5 mL) and slowly evaporated. For atomic force microscopy (AFM), transmission electron microscopy (TEM) study, the (P3HT−NH_3^+)-*b*-(PS−SO_3^-) thin film was treated by solvent annealing in a closed chamber exposed with a toluene steam at room temperature for 3 h.

Preparation of nanoporous P3HT. The (P3HT−NH_3^+)-*b*-(PS−SO_3^-) thin film on a mica (1 × 2 cm^2) was soaked into ethyl acetate/triethylamine (100/1, v/v, 5 mL) for 1 min to selectively remove PS and dried under vacuum overnight.

Measurements. Molecular weights (MWs) and PDIs were measured by GPC on a Jasco GULLIVER 1500 equipped with a pump, an absorbance detector (UV, λ = 254 nm), and three polystyrene gel columns based on a conventional calibration curve using polystyrene standards. Chloroform was used as a carrier solvent at a flow rate of 1.0 mL/min at room temperature. Proton nuclear magnetic resonance (^{1}H NMR) spectra were recorded on a Bruker DPX (300 MHz) in $CDCl_3$ calibrated to tetramethylsilane as an internal standard (δH 0.00). Matrix-assisted laser desorption ionization time-of-flight (MALDI−TOF) mass spectra were recorded on a Shimadzu AXMA-CFR mass spectrometer. The spectrometer was equipped with a nitrogen laser (337 nm) and with pulsed ion extraction. The operation was performed at an accelerating potential of 20 kV by linear-positive ion mode. A 10 μL of the sample polymer solution in THF (5 mg/mL) and a 100 μL of the matrix, 2,2′:5′2″-terthiophene (Aldrich) solution in THF (75 mg/mL) were well mixed. A 1 μL aliquot of the final solution was deposited onto a sample target plate and dried in air at room temperature. Mass values were calibrated by the three-point method with insulin plus H^+ at m/z 5734.62, insulin β plus H^+ at m/z 3497.96, and α-cyanohydroxycinnamic acid dimer plus H^+ at m/z 379.35. Fourier-transform infrared (FT-IR) spectra were measured by a Horiba FT-120 Fourier transform spectrophotometer. Differencial scanning calorimetry (DSC) analysis was performed with a Seiko EXSTAR 6000 DSC 6200. The samples were heated at 20 °C/min under nitrogen and the second thermograms were recorded. Calibrations were made using indium as a standard. Thermogravimetry (TGA) analysis was performed on a Seiko EXSTAR 6000 TG/DTA 6300 thermal analyzer at a heating rate of 10 °C/min. Ultraviolet−visible (UV−vis) absorption spectra of a polymer solution in chloroform and a thin film were recorded on a Jasco FP-750 spectrometer over a

Scheme 1. Synthetic Routes for (a) Regioregular P3HT by McCullough's Method and (b) P3HT−NH_2 by our Method

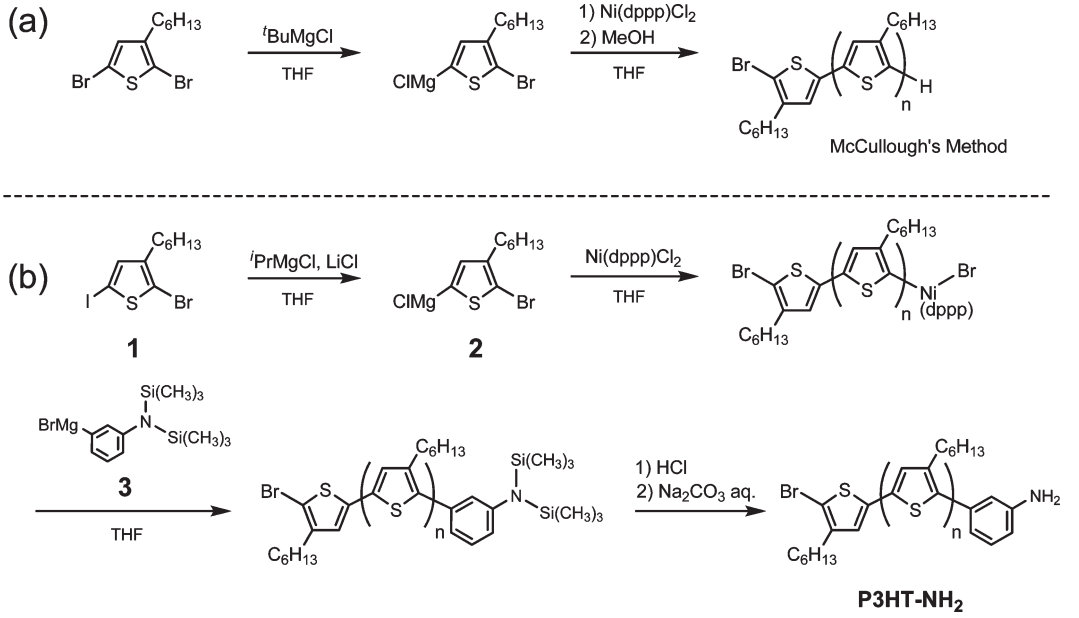

wavelength range of 250−800 nm. AFM phase images were taken with a SII-NT SPA 400 operating in a tapping mode. TEM images were obtained using a JEOL JEM-1010BS operated at 80 kV accelerating voltage. Block copolymer thin films were prepared by a drop casting onto a carbon support film on copper grid from a toluene solution (0.04 wt %), followed by solvent annealing with a toluene vapor at room temperature for 3 h. The films were then stained with a RuO_4 vapor for 10 min. Scanning electron microscopy (SEM) images were obtained by applying a Hitachi S-4500 electron microscope operated at an accelerating voltage of 15 kV. Grazing incidence X-ray scattering (namely grazing incidence small angle and wide-angle X-ray scattering (GISAXS and GIWAXS)) measurements were carried out at the 4C1 and 4C2 beamlines[30−34] of the Pohang Accelerator Laboratory at Pohang University of Science & Technology. Further, grazing incidence ultrasmall-angle X-ray scattering (GIUSAXS) measurements were carried out at the BW4 beamline of Deutsches Elektronen-Synchrotron (DESY) in Germany. The film samples, which were coated with a thickness of 35−200 nm on Si substrates, were measured at a sample-to-detector distance of 13670 mm (GIUSAXS), 2261.7 mm (GISAXS) and 126.6 mm (GIWAXS) using an X-ray radiation source of 0.138 nm wavelength and two-dimensional (2D) charge-coupled detectors (CCDs) (MAR USA and Roper Scientific). The samples were mounted on a homemade *z*-axis goniometer equipped with a vacuum. The incident angle α_i of the X-ray beam was set at 0.28° (GIUSAXS) and 0.16° (GISAXS and GIWAXS), which is between the critical angles of the films and the Si substrate ($\alpha_{c,f}$ and $\alpha_{c,s}$). All GIXS measurements were carried out at 25 °C. Each measurement was collected for 60 s (GISAXS and GIWAXS) and 300 s (GIUSAXS).

Results and Discussion

Synthesis of P3HT−NH_2 and PS−SO_3H. McCullough and co-workers reported a quasi-living GRIM polymerization of **2** initiated with Ni(dppp)Cl_2, starting from 2,5-dibromo-3-hexylthiophene which was treated with *tert*-butylmagnesium chloride via the Grignard exchange reaction (Scheme 1a).[35] As a result, the obtained P3HTs possess low PDIs in the range of 1.1−1.4. A subsequent end-functionalization reaction was also developed by them where quasi-living P3HT was reacted in situ with an excess of Grignard agents.[36,37] Indeed, a wide variety of functional groups have been introduced at P3HT chain end(s), including vinyl, allyl, alkyne, alkyl, aryl, phenol (pyrane-protected), formyl (acetal-protected), and aniline (dimethylsilyl-protected). They found that ω-end monosubstitution or α,ω-ends disubstitution depends on the nature of the Grignard reagents. When vinyl-, allyl-, and alkyne-containing Grignard reagents are used, monosubstitution takes place, whereas others result in disubstitution. The complexation between Grignard reagents and an Ni catalyst might be related to this selectivity. Interestingly, Grignard reagents consisting of a dimethylsilyl-protected aniline group brought about monosubstitution.

We have been interested in P3HT−NH_2 for a blend system with PS−SO_3H, so an end-functionalization reaction using 3-[bis(trimethylsilyl)amino]phenylmagnesium chloride was carried out under modified conditions. First, **1** and ^{i}PrMgCl were used instead of 2,5-dibromo-3-hexylthiophene and *tert*-butylmagnesium chloride, respectively, in order to further enhance the quantitative and selective Grignard exchange reaction at the 5-position and lower the PDIs (PDI = 1.08−1.13) without any shoulder from a GPC trace, as described by Yokozawa's group.[38] Second, our group employed an additive of lithium chloride (LiCl) in the reaction system, aiming at dissociation of the Grignard reagents and an increase in their reactivity in THF. Indeed, the yields and reproducibility of GRIM polymerization become higher in the presence of LiCl. The synthetic routes are depicted in Scheme 1b.

Monomer **2** was prepared by a stoichiometric Grignard exchange reaction of **1** with ^{i}PrMgCl at 0 °C for 30 min in the presence of LiCl in THF. The initiator, Ni(dppp)Cl_2, was then added and polymerization was carried out at room temperature for 10 min, followed by an in situ reaction with **3** for 10 min, which was always used in at least a 20-fold excess to the chain-end. Quenching the system with 5 N HCl(aq) deprotected the dimethylsilyl groups so as to directly generate an HCl salt of P3HT−NH_2. After neutralization with $NaCO_3$(aq), an aniline chain end could be regenerated. The obtained P3HT was characterized by GPC, NMR, and MALDI−TOF mass spectroscopy.

The results are summarized in Table 1. As the target molecular weight increases by increasing the feed ratio of monomer to initiator, the observed molecular weight

Table 1. Synthesis of Regioregular P3HT−NH_2

run	[M]/[I]	$\overline{M_n}$ (g/mol) calcd[a]	$\overline{M_n}$ (g/mol) GPC[b]	PDI[b]	convn (%)[c]
1	12	2000	1960	1.12	83
2	30	5000	5520	1.13	81
3	42	7000	7530	1.11	98
4	60	10 000	10 200	1.08	98
5	60	10 000	11 500	1.11	98
6	120	20 000	23 700	1.11	67

[a] Calculated from the feed ratio of monomer to initiator. [b] Determined by GPC using polystyrene standards. [c] Monomer conversion determined by GPC.

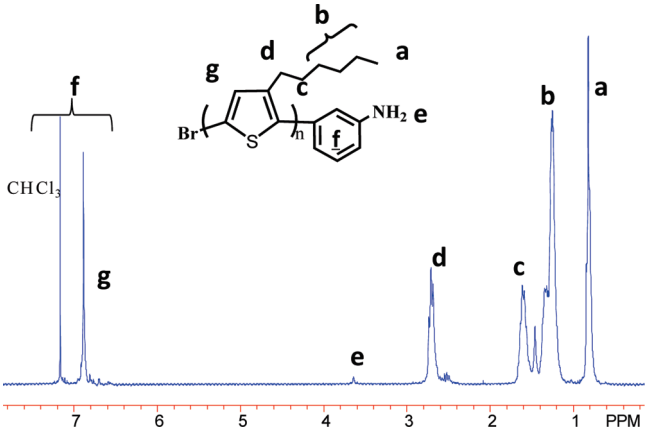

Figure 1. ^{1}H NMR spectrum of regioregular P3HT−NH_2 (run 1).

increases proportionally (see Supporting Information, Figure S1). The PDIs were low, in the range of 1.08−1.13, although they are not very accurate based on the relative molecular weights using polystyrene standards. The representative GPC curves of run 3 and 4 indicated sharp and unimodal peaks (see Supporting Information, Figure S2). The ^{1}H NMR spectra of the P3HT−NH_2 series show a characteristic resonance assignable to NH_2 protons at the end group with reasonable intensity (Figure 1 (run 1)). The head-to-tail regioregularity was determined from ^{1}H NMR to be more than 95% in all runs by comparing the signal intensity of the methylene protons next to the thiophene rings corresponding to head-to-tail structure and that of others. The representative MALDI−TOF mass spectrum of P3HT−NH_2 (run 2) is shown in Figure 2. The major series of signals with intervals corresponding to the monomer unit was found, assigning the α and ω-ends to bromo and aniline groups, respectively. No disubstituted products with aniline groups were found at all. For instance, the 13-mer of P3HT bearing bromo and aniline groups was observed at m/z = 2332.25, which is very close to the theoretical value (m/z = 2333.66 = 79.9 (Br) + 166.28 (monomer unit) × 13 (degrees of polymerization) + 92.12 (aniline)). A very minor series was also found, which is attributed to unfunctionalized P3HT having bromo and proton end groups. The end functionalities were calculated by comparing the signal intensities of both series[35] and they ranged from 85 to 92%. Thus, an efficient monosubstitution reaction was revealed to yield the expected well-defined regioregular P3HT−NH_2 without difficulty.

The precursor, PS−SO_3H, could also be successfully synthesized based on living anionic polymerization under the modified conditions of a previous paper.[39] Styrene was polymerized with *sec*-BuLi as the initiator in toluene at room temperature for 2 h and a THF (toluene/THF = 1/1, v/v) solution of DPE was added at −78 °C to tune the nucleophilicity of the chain end. The DPE-end-capped polystyryllithium

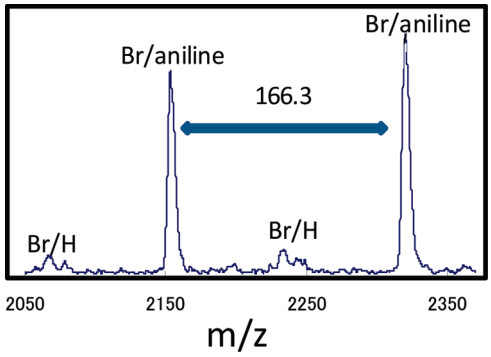

Figure 2. MALDI−TOF mass spectrum of regioregular P3HT−NH_2 (run 2).

Table 2. Synthesis of PS−SO_3H[a]

run	$\overline{M_n}$ (g/mol)[b]	PDI[b]	funct (%)[c]
7	1770	1.05	100
8	5460	1.03	100
9	12 500	1.03	100

[a] Yields of all polymers were 100%. [b] Determined by GPC using polystyrene standards. [c] Determined by TLC and acid/base titration.

was terminated with an excess of 1,3-propane sultone, followed by neutralization with a perchloric acid solution. The results are summarized in Table 2 and the representative GPC curve (run 7) showed extremely narrow distribution (see Supporting Information, Figure S3). The nearly 100% sulfo-functionality was confirmed by TLC and acid/base titration.

Synthesis of (P3HT−NH_3^+)-*b*-(PS−SO_3^-). The target block copolymers were syntheiszed by blending equimolar amounts of P3HT−NH_2 (run 3: $\overline{M_n}$ 7530) and PS−SO_3H (run 8: $\overline{M_n}$ 12 500) in a toluene solution (Scheme 2). The FT-IR spectra of P3HT−NH_2, PS−SO_3H and (P3HT−NH_3^+)-*b*-(PS−SO_3^-) are shown in Figure 3, parts a−c, respectively. The infrared absorption band at 1261 cm^{-1}, corresponding to the N−H deformation vibration observed in Figure 3a, disappears in Figure 3c as expected. Amine salts (−NH_3^+) should show a specific absorption band in the range of 1500−1600 cm^{-1}, but it overlaps with the S=O stretching vibration, unfortunately. On the other hand, (P3HT−NH_3^+)-*b*-(PS−SO_3^-) exhibited an absorption at 1215 cm^{-1} originating from the S=O stretching vibration of SO_3^-, which was not observed in Figure 3b. These results indicate the ion-bonding formation between the P3HT and PS segments.

Thermal and Optical Properties of (P3HT−NH_3^+)-*b*-(PS−SO_3^-). The thermal property of (P3HT−NH_3^+)-*b*-(PS−SO_3^-) ($\overline{M_n}$ = 7530 + 12 500) was investigated by DSC, and compared with a blend of unfunctionalized P3HT and PS−SO_3H (P3HT/PS−SO_3H) having similar molecular weight and composition. On heating run, the P3HT/PS−SO_3H blend shows two distinct transition temperatures, namely glass transition temperature T_g at 88 °C and melting temperature T_m at 221 °C, corresponding to PS−SO_3H and P3HT aggregated domains, respectively (Figure 4, dashed line). (P3HT−NH_3^+)-*b*-(PS−SO_3^-) also shows two transition temperatures (T_g at 90 °C and T_m at 215 °C) for both domains on heating, indicating a phase separation, but the intervals of both temperatures become somewhat closer compared to the P3HT/PS−SO_3H blend (Figure 4, solid line). This observation may be derived from a smaller phase-separated structure of (P3HT−NH_3^+)-*b*-(PS−SO_3^-) than that of P3HT/PS−SO_3H due to the block copolymer formation. A similar trend was also observed in a cooling scan with the exception that an extra small transition temperature peak was observed at 128 °C only

Scheme 2. Synthetic Route for (P3HT−NH_3^+)-*b*-(PS−SO_3^-)

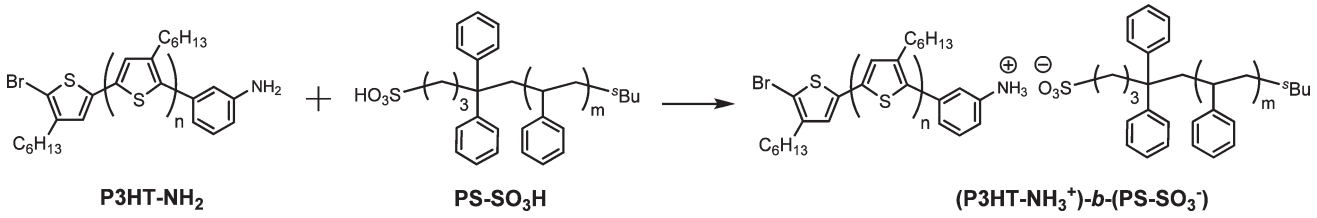

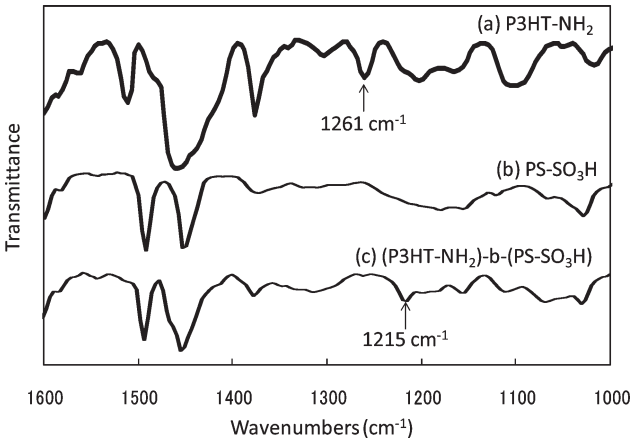

Figure 3. FT-IR spectra of (a) P3HT−NH_2, (b) PS−SO_3H and (c) (P3HT−NH_3^+)-*b*-(PS−SO_3^-) ($\overline{M_n}$ = 7350 + 12 500).

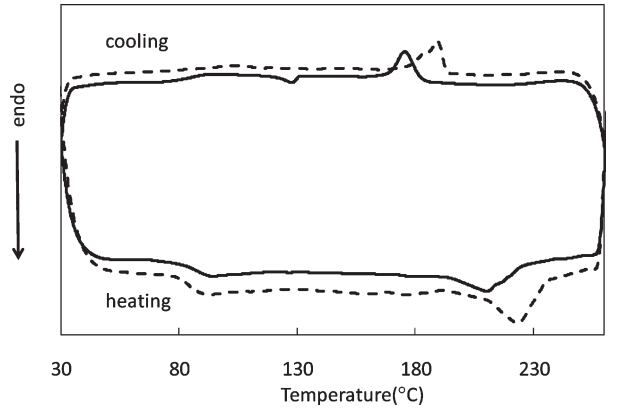

Figure 4. DSC thermograms of P3HT/PS−SO_3H blend (dashed line) and (P3HT−NH_3^+)-*b*-(PS−SO_3^-) ($\overline{M_n}$ = 7350 + 12 500) (solid line).

for (P3HT−NH_3^+)-*b*-(PS−SO_3^-) between T_g (90 °C, PS−SO_3^- domains) and crystallization temperature T_c (175 °C, P3HT−NH_3^+ domains), which might correspond to a fusion peak[40] of partially miscible P3HT−NH_3^+ and PS−SO_3^- domains. Indeed, this observation was not observed at all for the P3HT/PS−SO_3H blend, indicating totally immiscible domains.

The solution-state UV−vis spectra of (P3HT−NH_3^+)-*b*-(PS−SO_3^-) in *o*-dichlorobenzene are shown Figure 5. Maximum absorptions (λ_{max}) at 455 nm, assignable to a π- π* transition, were observed. In the solid state, the λ_{max} was bathochromically shifted to 560 nm compared to that in the solution state. In addition, the film showed a shoulder at around 611 nm, related to vibronic absorption, as seen in a pristine P3HT film, indicating a high degree of ordering in the polymer films, even though amorphous PS was mostly incorporated.

Morphological Structure of (P3HT−NH_3^+)-*b*-(PS−SO_3^-) Thin Films. To gain insight into the morphology, thin films of (P3HT−NH_3^+)-*b*-(PS−SO_3^-) ($\overline{M_n}$ = 7350 + 12 500) were prepared by drop casting onto mica substrates for microscopy analysis and silicon(Si) wafers for X-ray scattering analysis, followed by solvent annealing with toluene for 3 h. The film thickness was measured to be 150−200 nm by using α-stepper (model Dektak[3], Veeco Co., USA). In addition, films of the P3HT/PS−SO_3H blend were prepared on mica substrates as a reference and solvent-annealed in the same way as the (P3HT−NH_3^+)-*b*-(PS−SO_3^-) films were treated.

The films were first examined by AFM. As can be seen in Figure 6a, the blend film shows macrophase separation without any nano-ordered morphology. The (P3HT−NH_3^+)-*b*-(PS−SO_3^-) films also show macrophase separation (Figure 6b). However, the block copolymer film additionally reveals continuous nanofibril structures (Figure 6b). The other (P3HT−NH_3^+)-*b*-(PS−SO_3^-) block copolymer samples, which have different P3HT contents (P3HT: 52% (run 5 + run 9) and 65 wt % (run 4 + run 8)), also similar nanofibril-like morphology (Figure 6, parts c and d). The block copolymer films were further investigated by TEM. A representative TEM image of a (P3HT−NH_3^+)-*b*-(PS−SO_3^-) ($\overline{M_n}$ = 7350 + 12 500) thin film is depicted in Figure 7, indicating that nanofibrils and their bundle structure were formed in the film. Moreover, the TEM image shows that the nanofabrils fill the sample as the minor fraction in area. As discussed earlier, the DSC study indicates that the P3HT−NH_3^+ blocks undergo ordering while the PS−SO_3^- blocks remain amorphous. Therefore, the AFM and TEM results together with the DSC result confirm that that such the nanofibrils were made of the P3HT−NH_3^+ block, which is the minor component of the block copolymer. Further, taking the TEM and DSC results into account, the bright and dark areas in Figure 6b can be assigned as the P3HT−NH_3^+ and PS−SO_3^- domains, respectively. From the AFM and TEM images, the nanofibrils were estimated to have a width of 15−18 nm and a length of few hundred nanometers. Such the nanofibril structures are similar to those reported previously for covalent-bonded P3HT-*b*-PS films.[16]

Taking the above AFM and TEM results into account, the (P3HT−NH_3^+)-*b*-(PS−SO_3^-) films were further examined by synchrotron GIXS analysis. Figure 8 shows representative GIUSAXS and GISAXS data measured for the block copolymer films. The in-plane profiles of the GIUSAXS and GISAXS data, which were extracted along the $2\theta_f$ direction at α_f = 0.175° from the 2D GIUSAXS image (Figure 8a) and at α_f = 0.160° from the 2D GISAXS image (Figure 8, parts b and c), were plotted together in Figure 8d. As can be seen in the figure, a scattering peak is distinguishable around $2\theta_f$ = 0.49° although it is weak and broad. This peak is apparently more distinguishable for the 35 nm thick film than for the 200 nm thick film. The *d*-spacing of the scattering peak is determined to be 16.14 nm, which is comparable to those estimated from the AFM and TEM images (Figures 6b and 7). Taking the TEM result into account, this *d*-spacing can be assigned to the mean interdistance between the nanofibrils in the P3HT−NH_3^+ fibril bundle (i.e., phase-separated P3HT−NH_3^+ domain). In addition, another scattering peak is

suspected around at $2\theta_f = 0.0205°$ (Figure 8d), which is very weak and broad. Its *d*-spacing value is estimated to be 385.9 nm. This *d*-spacing value is quite large, indicating that the very weak scattering peak is attributed to the mean interdistance between the phase-separated P3HT−NH_3^+ and PS−SO_3^- domains in the film; these P3HT−NH_3^+ and PS−SO_3^- domains in large scale were confirmed in the TEM image (Figure 7). Moreover, the appearance of such the very weak, broad scattering peak in the low angle indicates that the electron density difference between the macroscopic P3HT−NH_3^+ and PS−SO_3^- domains formed in the film is very low and the sizes of the domains are in broad distribution.

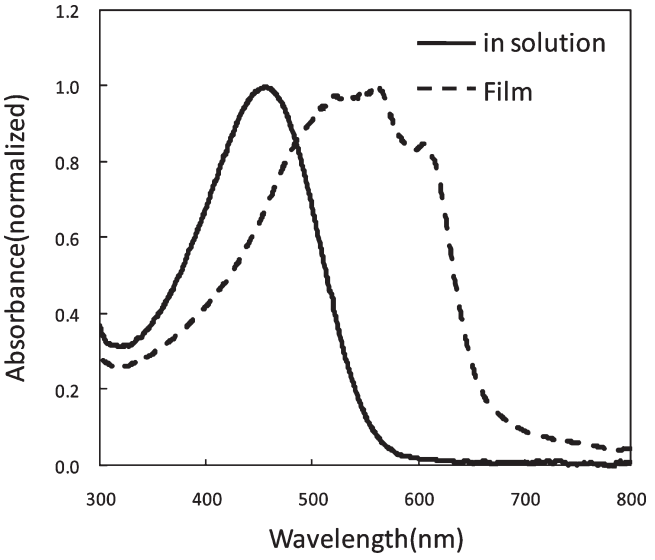

Figure 5. UV−vis spectra of (P3HT−NH_3^+)-*b*-(PS−SO_3^-) ($\overline{M_n}$ = 7350 + 12 500) in solution and film states.

Figure 9 shows representative GIWAXS patterns of the films (35 and 200 nm thick) measured at $\alpha_i = 0.16°$. Several strong scattering spots clearly appear along the α_f direction at $2\theta_f = 0°$ (Figure 9a−c). Their relative scattering vector lengths from the specular reflection position are 1, 2 and 3, indicating that the scattering spot in the low angle region is the first-order reflection and the other two spots are the second- and third-order reflections of the first-order one. Therefore, the scattering results indicate that layered structure is formed in the P3HT−NH_3^+ domains, whose layers are stacked normal to the film plane. From these scattering spots, the *d*-spacing is determined to be 1.65 nm, which corresponds to the single molecular layer thickness of the layer structures formed in the P3HT−NH_3^+ domains. The scattering spots are apparently much sharper for the 35 nm thick film than for the 200 nm thick film; in fact, those of the 200 nm thick film are arc-like (Figure 9). These results indicate that in the thinner film the molecular layer stacks of the P3HT−NH_3^+ domains are more preferentially oriented in the out-of-plane of the film, compared to those in the thicker film.

In addition to the scattering spots, the block copolymer films reveal isotropic and anisotropic scattering rings over the range of 13−23° (Figure 9). The isotropic ring centered at

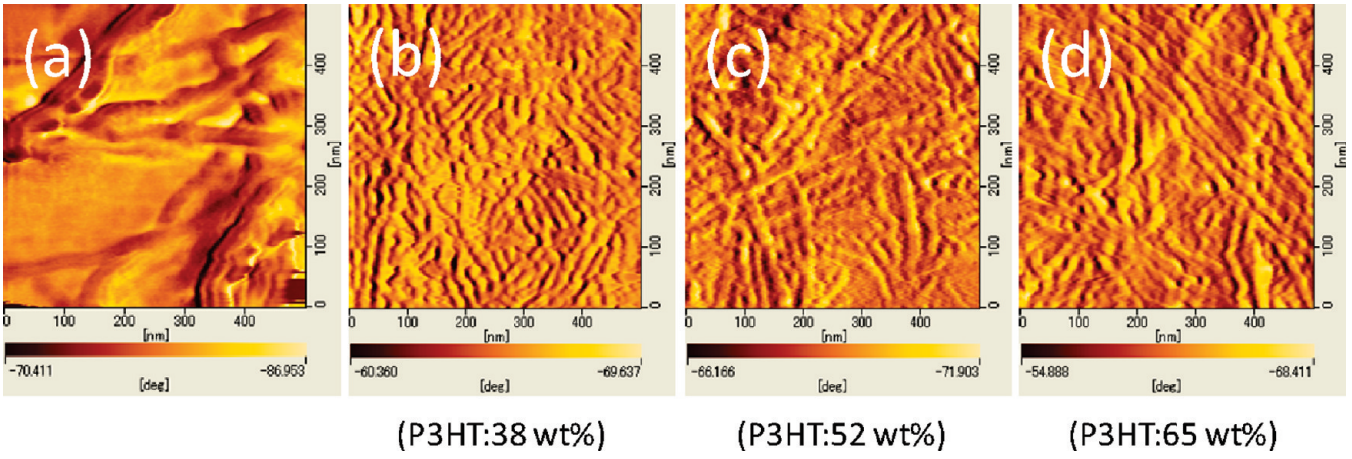

Figure 6. Tapping mode AFM phase images of (a) a blend film of unfunctionalized P3HT and PS−SO_3H, and (b−d) (P3HT−NH_3^+)-*b*-(PS−SO_3^-) films treated by solvent annealing with toluene at room temperature for 3 h.

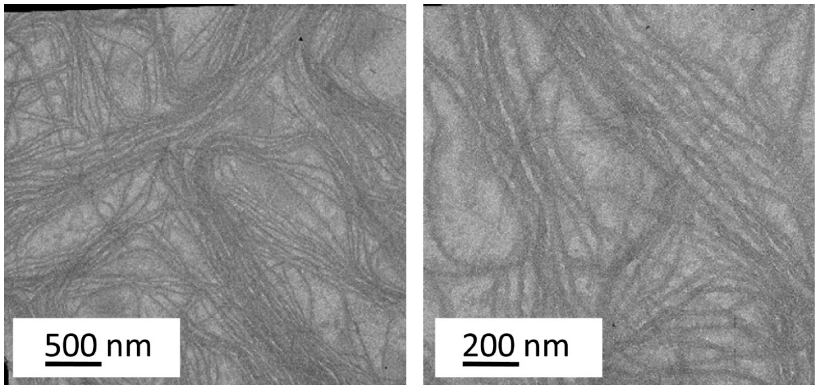

Figure 7. TEM images of a (P3HT−NH_3^+)-*b*-(PS−SO_3^-) ($\overline{M_n}$ = 7350 + 12 500) thin film.

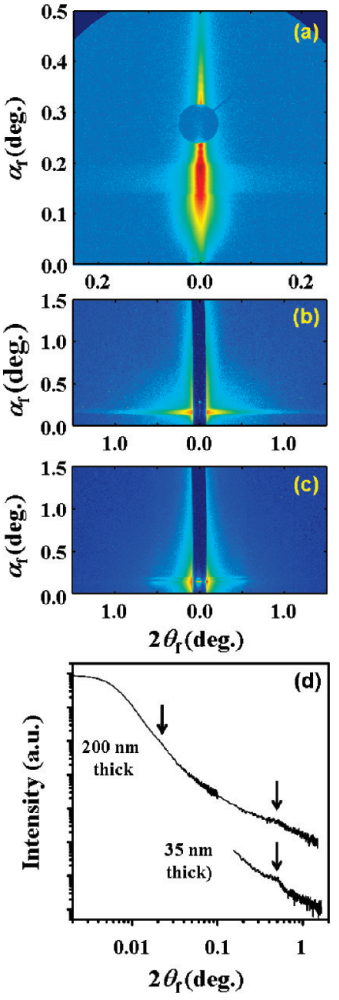

Figure 8. GIUSAXS and GISAXS data measured for films of (P3HT−NH_3^+)-*b*-(PS−SO_3^-) ($\overline{M}_n$ = 7350 + 12 500): (a) 2D GIUSAXS pattern measured at α_i = 0.28° for the 200 nm thick film; (b) 2D GISAXS pattern measured at α_i = 0.16° for the 200 nm thick film; (c) 2D GISAXS pattern measured at α_i = 0.16° for the 35 nm thick film; (d) in-plane scattering profiles extracted along the $2\theta_f$ direction at α_f = 0.175° from the 2D GIUSAXS pattern (a) and at α_f = 0.160° from the 2D GISAXS patterns (b and c).

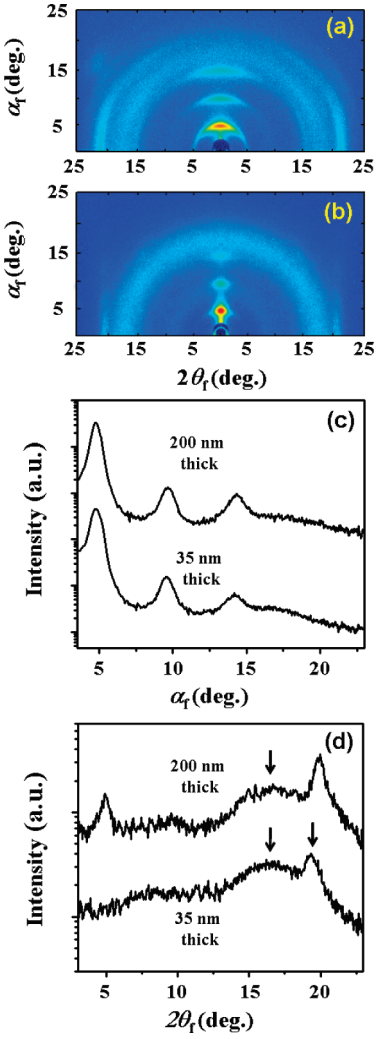

Figure 9. GIWAXS data measured for films of (P3HT−NH_3^+)-*b*-(PS−SO_3^-) ($\overline{M}_n$ = 7350 + 12 500): (a) 2D GIWAXS pattern measured at α_i = 0.16° for the 200 nm thick film; (b) 2D GIWAXS pattern measured at α_i = 0.16° for the 35 nm thick film; (c) out-of-plane scattering profiles extracted along the α_f direction at $2\theta_f$ = 0.0° from the scattering patterns in parts a and b; (d) in-plane scattering profiles extracted along the $2\theta_f$ direction at α_f = 0.0° from the scattering patterns in parts a and b.

$2\theta_f$ = 16.40° is very broad and its *d*-spacing is determined to be 0.48 nm. This *d*-spacing value corresponds to the mean interdistance of the PS−SO_3^- block chains as well as that of phenyl side groups. The *d*-spacing value also corresponds to the mean interdistance of the P3HT−NH_3^+ block chains. Thus, such the peak broadness is a result of the three different origins of interdistances in partial or full overlaps. On the other hand, the anisotropic scattering ring centered at $2\theta_f$ = 19.34° is much sharper than the isotropic ring at $2\theta_f$ = 16.40° (Figure 9). Its *d*-spacing value is determined to be 0.41 nm, which is slightly smaller than the interdistances of the block chains and the phenyl side groups. The anisotropic characteristic is much stronger for the thinner film than the thicker film (Figure 9). Taking into account the molecular multilayer structure discussed above, the results collectively indicate that the anisotropic ring peak is originated from the mean interdistance of the P3HT−NH_3^+ blocks' *n*-hexyl side groups ordered in the out-of-plane of the film.

Preparation of Nanoporous P3HT−NH_2 Films. In order to create novel nanoporous P3HT−NH_2 films, the selective etching of PS−SO_3^- domains from (P3HT−NH_3^+)-*b*-(PS−SO_3^-) film ($\overline{M}_n$ = 7530 + 12 500) via a wet process using ethyl acetate/triethylamine (100/1, v/v) was performed by exploiting pH-stimulating ionic interaction between P3HT−NH_2 and PS−SO_3H blocks. Ethyl acetate and triethylamine play important roles in the selective solvent for PS and the cleavage of amine-sulfonic acid interaction, respectively. After the solvent etching process, the characteristic aromatic absorption at 3000−3080 cm^{-1} of the PS−SO_3H blocks completely disappeared in the FT-IR spectrum of the resulting film, which is indicative of the complete removal of the PS−SO_3H blocks (see Figure 10). The AFM (topographic image) and SEM images of the nanoporous films are shown in Figures 11 and 12, respectively. For the as-cast (P3HT−NH_3^+)-*b*-(PS−SO_3^-) film, the topographic views show little change in the surface across a scan area with a roughness of 35 nm (Figure 11a). On the contrary, after removal of the PS−SO_3^+ domains, the formation of nanoporosity in the thin film surface was observed with a roughness of 70 nm (Figure 11b). Unfortunately, the remaining P3HT−NH_2 domains partially tended to collapse, probably due to the wet process and high aspect ratio more than 5 (domain width, 15−18 nm; film thickness, 100 nm). SEM images also revealed the nanoporous structures of P3HT−NH_2 thin

films. Although nanodomains were maintained in some areas, collapsed P3HT−NH_2 domains could also be found (Figure 12), which agrees with the AFM observations. This issue may come from the surface tension force during liquid evaporation from the film. Alignment and fixation of nanoporous P3HT−NH_2 domains without collapsed structures are now under investigation. A dry etching process, utilizing supercritical solvents such as CO_2 and *n*-butane, could be a strong strategy to solve the issue of domain collapse.[41]

With the AFM and SEM results, the nanoporous films were further investigated by GIX analysis. Figure 13 displays

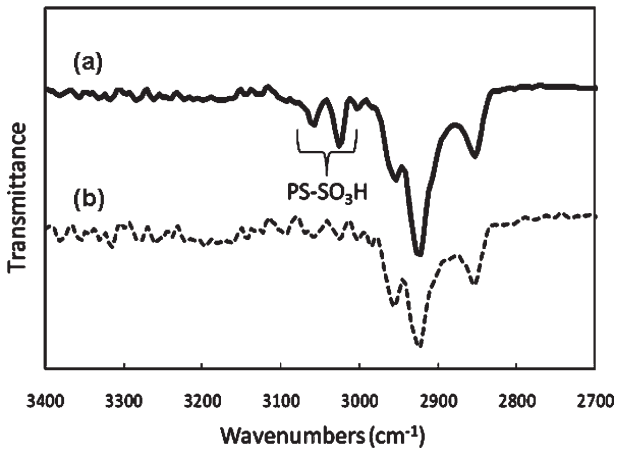

Figure 10. FT-IR spectra of a film of (P3HT−NH_3^+)-*b*-(PS−SO_3^-) ($\overline{M_n}$ = 7530 + 12 500) (which was treated by solvent annealing with toluene at room temperature for 3 h): (a) before and (b) after removal of PS−SO_3^- domains via selective chemical etching.

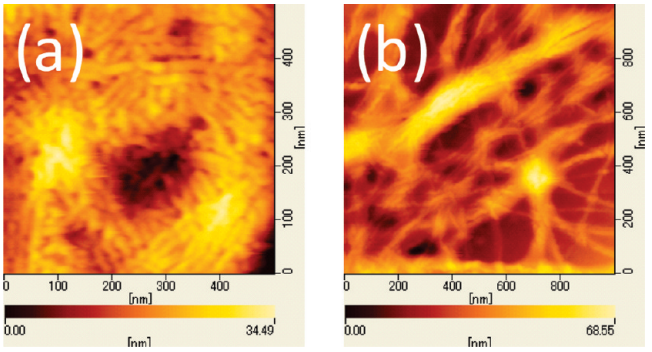

Figure 11. AFM topographic images of a film of (P3HT−NH_3^+)-*b*-(PS−SO_3^-) ($\overline{M_n}$ = 7530 + 12 500) (which was treated by solvent annealing with toluene at room temperature for 3 h): (a) before and (b) after removal of PS−SO_3^- domains via selective chemical etching.

representative 2D GIUSAXS and GISAXS patterns and their in-plane and out-of-plane scattering profiles. In the in-plane scattering profile (Figure 13c), a scattering peak is clearly distinguished around $2\theta_f = 0.0205°$ (*d*-spacing = 385.9 nm). Its *d*-spacing value is equivalent to the mean interdistance between the phase-separated P3HT−NH_3^+ and PS−SO_3^- domains in the film. The scattering peak is broad and, however, its intensity apparently is much stronger, compared to that before etching. Taking the AFM and SEM results into account, such the intensity enhancement in the scattering peak is attributed to the large electron density contrast between the large pores (voids) (which are the footmarks by the removal of PS−SO_3^- domains via the selective chemical etching) and the remained P3HT−NH_2 domains. The determined *d*-spacing value indicates that the removal process of the PS−SO_3^- domains via selective chemical etching does not influence significantly the mean interdistance of the phase separated P3HT−NH_3^+ domains. In addition, another scattering peak is suspected around $2\theta_f$ = 0.58° although the peak is very broad and weak (Figure 13c). Its *d*-spacing value is determined to be 13.6 nm, which is slightly smaller than that before etching. This result indicates that the nanofibrils in the remained P3HT−NH_2 domains were slightly collapsed through selective etching of the PS−SO_3^- domains from the film, which is consistent with the AFM and SEM results.

Figure 13d displays the out-of-plane scattering profile of the film before and after selective etching; here it is noted that the nonsignal regions over 0.24−0.32° was attributed to the beam-stopper used. A Yoneda wing is observed below 0.2° for the nonetched film and below 0.1° for the etched film. In comparison, the Yoneda wing is relatively less distinguished for the etched film, which might be due to the relatively rougher surface of the film. From the observed Yoneda wings, the critical angle α_c is determined to 0.139° for the nonetched film and 0.097° for the etched film (i.e., nanoporous film). From the critical angles, the electron density ρ_e is estimated to be 344 nm^{-3} for the nonetched film and 168 nm^{-3} for the etched film by using a relation $\rho_e = \pi\alpha_c^2/r_e\lambda^2$ where r_e is the classical radius (2.818×10^{-15} *m*) of electron and λ is the wavelength of the used X-ray beam. Further, from the obtained electron densities, the etched film (nanoporous film) is determined to have a porosity of 51.2%.

Figure 14 shows a representative 2D GIWAXS pattern of the etched films and its in-plane and out-of-plane scattering profiles. The scattering data of the etched film resembles that of the nonetched film. However, the isotropic ring centered at $2\theta_f = 16.40°$ is weakened very much, which was caused by the removal of the PS−SO_3^- domains via selective etching. These scattering results confirm that the remained parts in the etched film are the P3HT−NH_2 domains. Moreover, the

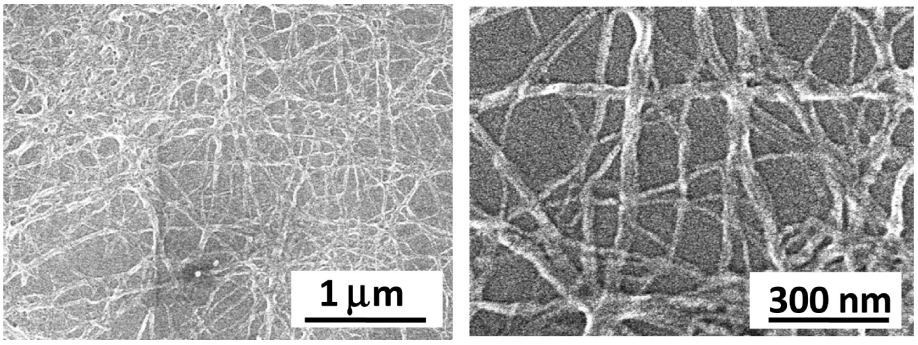

Figure 12. SEM images of the nanoporous film obtained from a film of (P3HT−NH_3^+)-*b*-(PS−SO_3^-) ($\overline{M_n}$ = 7530 + 12 500) (which was treated by solvent annealing with toluene at room temperature for 3 h) after removal of PS−SO_3^- domains via selective chemical etching.

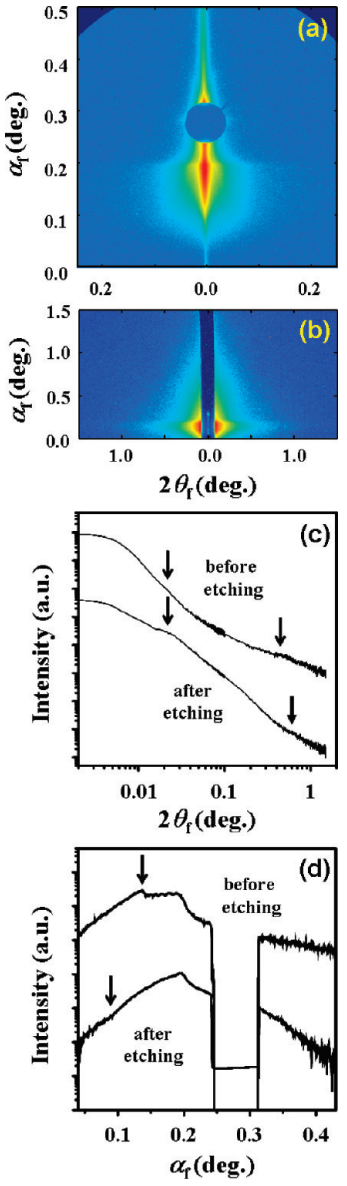

Figure 13. GIUSAXS and GISAXS data of the nanoporous film obtained from a film of (P3HT−NH_3^+)-*b*-(PS−SO_3^-) ($\overline{M_n}$ = 7530 + 12 500) (which was treated by solvent annealing with toluene at room temperature for 3 h) after removal of PS−SO_3^- domains via selective chemical etching: (a) 2D GIUSAXS pattern measured at α_i = 0.28°; (b) 2D GISAXS pattern measured at α_i = 0.16°; (c) in-plane scattering profiles extracted along the $2\theta_f$ direction at α_f = 0.175° from the 2D GIUSAXS pattern (a) and at α_f = 0.160° from the 2D GISAXS pattern (b), which is compared with those before etching; (d) out-of-plane scattering profile extracted along the α_f direction at $2\theta_f$ = 0.08° from the 2D GIUSAXS pattern (a), which is compared with that before etching.

remained P3HT−NH_2 domains still retain the molecular layer structure formed in the film before etching. However, the scattering spots along the meridian line became more arc-like and the anisotropy of the scattering peak centered at $2\theta_f$ = 19.34° was slightly reduced and weakened, compared to those of the nonetched film. These results indicate that the orientation of the molecular layer structure was slightly disturbed through the chemical etching process.

From the above structural analysis results, the PS−SO_3^- domains were successfully removed out from the film by the selectively wet chemical etching process but the P3HT−NH_2 domains were retained in the nanofibrils and their bundle

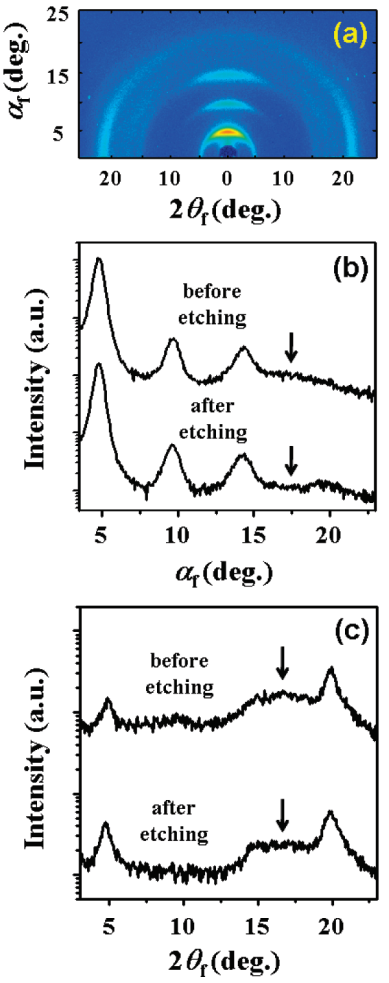

Figure 14. GIWAXS data of the nanoporous film obtained from a film of (P3HT−NH_3^+)-*b*-(PS−SO_3^-) ($\overline{M_n}$ = 7530 + 12 500) (which was treated by solvent annealing with toluene at room temperature for 3 h) after removal of PS−SO_3^- domains via selective chemical etching: (a) 2D GIWAXS pattern measured at α_i = 0.16°; (b) out-of-plane scattering profiles extracted along the α_f direction at $2\theta_f$ = 0.0° from the scattering patterns in part a, compared with that before etching; (c) in-plane scattering profiles extracted along the $2\theta_f$ direction at α_f = 0.0° from the scattering patterns in part a, compared with that before etching.

which have ordered molecular layer structure. Consequently, the nanoporous structure of P3HT−NH_2 polymer only was successfully constructed.

Conclusions

This report described the first example of the facile preparation of nanoporous P3HT films via a template system of block copolymers consisting of P3HT and PS segments. The system employs pH-sensitive ionic interaction between both segments for intentional cleavage after microphase separation. First, well-defined chain-end-functionalized regioregular P3HT−NH_2 and PS−SO_3H could be successfully synthesized based on quasi-living GRIM and living anionic polymerization, respectively. We were also successful in synthesizing novel ion-bonded block copolymers, (P3HT−NH_3^+)-*b*-(PS−SO_3^-), simply by blending P3HT−NH_2 with PS−SO_3H in toluene. Tapping-mode AFM phase and TEM images of the block copolymer films indicated the self-assembly of these films, which show nanofibril structures 15−18 nm in width and a few hundred nanometers in length. GIUSAXS and GISAXS experiments also confirmed the microphase separation of the P3HT−NH_3^+ and PS−SO_3^- domains.

In addition, the *d*-spacing values in the P3HT−NH_3^+ arrangements were determined from the GIWAXS pattern. The target nanoporous P3HT−NH_2 films were obtained by selective removal of the PS−SO_3^-domains by a wet process with ethyl acetate/triethylamine, as confirmed by AFM, SEM and GIXS analysis, although partially collapsed structures were also found.

Acknowledgment. We would like to thank the Japan Society for the Promotion of Science (JSPS) for mainly supporting this work by KAKENHI (20850014). The technical support of Mr. Ryohei Kikuchi, Center for Advanced Materials Analysis, Tokyo Institute of Technology, for the TEM operation is gratefully acknowledged. M.R. appreciates the financial support from the National Research Foundation of Korea (Center for Electro-Photo Behaviors in Advanced Molecular Systems) and the Ministry of Education, Science & Technology (MEST) of Korea (BK21 Program and World Class University Program). The synchrotron GIXS measurements at Pohang Accelerator Laboratory were supported by the MEST, POSCO and POSTECH Foundations.

Supporting Information Available: Figures S1, S2, and S3, respectively, showing a plot of $[M]_0/[I]_0$ versus M_n values of P3HT−NH_2 samples, GPC UV curves of regioregular P3HT−NH_2 samples, and GPC UV curve of PS−SO_3H. This material is available free of charge via the Internet at http://pubs.acs.org.

References and Notes

(1) Jenekhe, S. A.; Chen, X. L. *Science* **1999**, *283*, 372–375.
(2) Klok, H. A.; Lecommandoux, S. *Adv. Mater.* **2001**, *13*, 1217–1229.
(3) Lee, M.; Cho, B. -K.; Zin, W. -C. *Chem. Rev.* **2001**, *101*, 3869–3892.
(4) Lee, M.; Yoo, Y. -S. *J. Mater. Chem.* **2002**, *12*, 2161.
(5) Lim, Y. -B.; Moon, K. -S.; Lee, M. *J. Mater. Chem.* **2008**, *18*, 2909.
(6) Hiorns, R. C.; Holder, S. J. *Polym. Int.* **2009**, *58*, 323–329.
(7) Lee, J. S.; Hirao, A.; Nakahama, S. *Macromolecules* **1988**, *21*, 274–276.
(8) Lee, J. S.; Hirao, A.; Nakahama, S. *Macromolecules* **1989**, *22*, 2602–2606.
(9) Hillmyer, M. A. *Adv. Polym. Sci.* **2005**, *190*, 137–181.
(10) Olson, D. A.; Chen, L.; Hillmyer, M. A. *Chem. Mater.* **2008**, *20*, 869–890.
(11) Darling, S. B. *Energy Environ. Sci.* **2009**, *2*, 1266–1273.
(12) Segalman, R. A.; McCulloch, B.; Kirmayer, S.; Urban, J. J. *Macromolecules* **2009**, *42*, 9205–9216.
(13) Boudouris, B. W.; Frisbie, C. D.; Hillmyer, M. A. *Macromolecules* **2008**, *41*, 67–75.
(14) Botiz, I.; Darling, S. B. *Macromolecules* **2009**, *42*, 8211–8217.
(15) Sivanandan, K.; Chatterjee, T.; Treat, N.; Kramer, E. J.; Hawker, C. J. *Macromolecules* **2010**, *43*, 233–241.
(16) Iovu, M. C.; Craley, C. R.; Jeffries-El, M.; Krankowski, A. B.; Zhang, R.; McCullough, R. D. *Macromolecules* **2007**, *40*, 4733–4735.
(17) Iovu, M. C.; Jeffries-El, M.; Sheina, E. E.; Cooper, J. R.; McCullough, R. D. *Polymer* **2005**, *46*, 8582–8586.
(18) Higashihara, T.; Ohshimizu, K.; Hirao, A.; Ueda, M. *Macromolecules* **2008**, *41*, 9505–9507.
(19) Higashihara, T.; Ueda, M. *Macromolecules* **2009**, *42*, 8794–8800.
(20) Higashihara, T.; Ueda, M. *React. Funct. Polym.* **2009**, *69*, 457–462.
(21) Dai, C. A.; Yen, W. C.; Ho, C. C.; Su, W. F. *J. Am. Chem. Sci.* **2007**, *129*, 11036–11038.
(22) Horrion, J.; Jérôme, R.; P. Teyssié, T. *J. Polym. Sci., Polym. Lett. Ed.* **1986**, *24*, 69.
(23) Horrion, J.; Jérôme, R.; P. Teyssié, T. *J. Polym. Sci., Polym. Lett. Ed.* **1990**, *28*, 153.
(24) Russell, T. P.; Jérôme, R.; Charlier, P.; Foucart, M. *Macromolecules* **1988**, *21*, 1709–1717.
(25) Iwasaki, K.; Hirao, A.; Nakahama, S. *Macromolecules* **1993**, *26*, 2126–2131.
(26) Pispas, S.; Floudas, G.; Pakula, T.; Lieser, G.; Sakellariou, S.; Hadjichristidis, N. *Macromolecules* **2003**, *36*, 759–763.
(27) Hirao, A.; Karasawa, Y.; Higashihara, T.; Zhao, Y.; Sugiyama, K. *Design. Monom. Polym.* **2004**, *7*, 647–660.
(28) Sugiyama, K.; Karasawa, Y.; Higashihara, T.; Zhao, Y.; Hirao, A. *Monatsh. Chem.* **2006**, *137*, 869–880.
(29) Yokoyama, A.; Miyakoshi, R.; Yokozawa, T. *Macromolecules* **2004**, *37*, 1169–1171.
(30) Lee, B.; Park, Y. -H.; Hwang, Y. T.; Oh, W.; Yoon, J.; Ree, M. *Nat. Mater.* **2005**, *4*, 147–150.
(31) Lee, B.; Oh, W.; Hwang, Y.; Park, Y. -H.; Yoon, J.; Jin, K. S.; Heo, K.; Kim, J.; Kim, K. -W.; Ree, M. *Adv. Mater.* **2005**, *17*, 696–701.
(32) Yoon, J.; Kim, K. W.; Kim, J.; Heo, K.; Jin, K. S.; Jin, S.; Shin, T. J.; Lee, B.; Rho, Y.; Ahn, B.; Ree, M. *Macromol. Res.* **2008**, *16*, 575.
(33) Kim, G.; Park, S.; Jung, J.; Heo, K.; Yoon, J.; Kim, H.; Kim, I. J.; Kim, J. R.; Lee, J. I.; Ree, M. *Adv. Funct. Mater.* **2009**, *19*, 1631–1644.
(34) Yoon, J.; Jin, S.; Ahn, B.; Rho, Y.; Hirai, T.; Maeda, R.; Hayakawa, T.; Kim, J.; Kim, K, -W.; Ree, M. *Macromolecules* **2008**, *41*, 8778–8784.
(35) Iovu, M. C.; Sheina, E. E.; McCullough, R. D. *Macromolecules* **2005**, *38*, 8649–8656.
(36) Jeffries-El, M.; Sauvé, G.; McCullough, R. D. *Adv. Mater.* **2004**, *16*, 1017–1019.
(37) Jeffries-El, M.; Sauvé, G.; McCullough, R. D. *Macromolecules* **2005**, *38*, 10346–10352.
(38) Miyakoshi, R.; Yokoyama, A.; Yokozawa, T. *J. Am. Chem. Soc.* **2005**, *127*, 17542–17547.
(39) Quirk, R. P.; Yin, J. *J. Polym. Sci., Part A* **1992**, *30*, 2349–2355.
(40) Cho, J. C.; Cheng, G.; Feng, D.; Faust, R.; Richard, R.; Schwarz, M.; Chan, K.; Boden, M. *Biomacromolecules* **2006**, *7*, 2997–3007.
(41) Botiz, I.; Martinson, A. B. F.; Darling, S. B. *Langmuir* ASAP (DOI: 10.1021/la904515z).